Enhanced carrier extraction of a-Si/c-Si solar cells by nanopillar-induced optical modulation

2014 Nanotechnology 25 135202

(http://iopscience.iop.org/0957-4484/25/13/135202)

IOP Publishing Nanotechnology
Nanotechnology **25** (2014) 135202 (6pp) doi:10.1088/0957-4484/25/13/135202

Enhanced carrier extraction of a-Si/c-Si solar cells by nanopillar-induced optical modulation

Yang Zeng, Hong Liu, Qinghao Ye and Wenzhong Shen

Institute of Solar Energy, and Key Laboratory of Artificial Structures and Quantum Control (Ministry of Education), Department of Physics, Shanghai Jiao Tong University, Shanghai 200240, People's Republic of China

E-mail: wzshen@sjtu.edu.cn

Received 30 September 2013, revised 20 January 2014
Accepted for publication 27 January 2014
Published 28 February 2014

Abstract

We demonstrate improved short-wavelength internal quantum efficiency (IQE) of a-Si/c-Si heterojunction (HJ) solar cells with a surface nanopillar (NP) array via simulation. The gain in IQE is attributed to the light-field modulation caused by the cavity resonance inside the NPs, in which the light energy is effectively localized within the c-Si bulk rather than the a-Si layer. The average IQE in the short-wavelength range (330–450 nm) is enhanced from 43.94% to 62.88% by the optimal NP array, with a maximum IQE of 80.98% at $\lambda = 400$ nm. The resulting current gain is over 38.25% compared to a planar HJ cell in this wavelength range, showing a well suppressed recombination-induced current loss. This light-management scheme may also find applications in other types of cells.

Keywords: carrier extraction, heterojunction solar cell, IQE, nanopillar array, optical modulation, resonance

(Some figures may appear in colour only in the online journal)

1. Introduction

In recent years, the application of nanostructures to a solar cell's surface has been extensively investigated as part of the continuous effort to increase the cell's absorption [1, 2]. However, this only focuses on one specific aspect of maximizing the cell's current, since for many cell constructs, higher optical absorption alone does not guarantee higher current [3, 4]. A more precise formula would take carrier recombination into account, and the short-circuit current of a solar cell is expressed as

$$I_{sc} = e\int_0^{\lambda_{max}} [1 - R(\lambda) - T(\lambda)] \times \mathrm{IQE}(\lambda) \times N(\lambda)\,\mathrm{d}\lambda$$

where R and T denote the reflectance from and transmittance through the solar cell, IQE (internal quantum efficiency) denotes the proportion of photogenerated carriers that can be effectively extracted and N denotes the photon flux per wavelength. The first two terms on the right of the above equation also represent the two most common approaches for solar cell efficiency improvement: (1) improvement of the optical absorption ($A = 1 - R - T$) by employing rationally designed surface structures and (2) improvement of the electrical transport and carrier extraction (IQE) by optimizing the properties of the cell's materials. Nevertheless, these two methods are both bounded by intrinsic limits. For optical absorption, the highest possible absorption rate is unity. For electrical transport, high recombination loss of the carriers in the a-Si layer is inevitable. These issues seem to have set an upper limit for solar cell efficiency which it is difficult to overcome by the traditional use of surface nanostructures.

However, as we will show in this paper, the nanostructures do have the potential to improve the cell efficiency beyond this limit. Their ability to modulate the surface light field might be a key factor in solving the second issue, i.e., the recombination loss. This is due to the fact that the electrical loss is not only influenced by the electrical property of the material, but also

by the local-carrier-generation rate (due to the dependence of the recombination rate on the density of the local excess carriers), which can be modified by taking advantage of the sub-wavelength feature of the nanostructures. In the following, we will take the amorphous (a-) Si/crystalline (c-) Si heterojunction (HJ) solar cell (which suffers significantly from a low IQE (<50%) in the short-wavelength range ($\lambda \sim 400$ nm) due to the severe recombination in the heavily doped a-Si window layer [4], with a total current loss as high as 2–4 mA cm^{-2}) as an example and demonstrate this new optical method to improve the spectral response (IQE) of the cell. In the simulation, we will show that with carefully tuned dimensions, a surface nanopillar (NP) array can not only provide optical anti-reflection (AR) as commonly known, but also strongly enhance the carrier extraction by shifting the absorption front towards a c-Si-favoring paradigm. In the discussion, we will illustrate the gain in both optics (anti-reflection) and electrics (IQE) in a comparative way and further reveal the physical link between them, i.e. the cavity resonance. Finally, we demonstrate an IQE increase of 71% at certain wavelengths and a current gain of over 38% for the wavelength range of 330–450 nm, indicating a well suppressed electrical loss by optical modulation. These results suggest a new approach to improve the efficiencies of certain types of cells.

2. Simulation

The schematic drawings of a simulated NP HJ cell and its structural unit are shown in figures 1(a) and (b), respectively. The cell consists of (from bottom to top) an 80 nm-thick ITO rear contact (omitted from the figure for clarity), a c-Si substrate with an NP pattern on the front surface, a 10 nm-thick a-Si layer deposited onto the c-Si substrate and an 80 nm-thick ITO front contact coated around the a-Si layer (omitted from the figure for clarity). We employ the finite-difference time-domain (FDTD) method to obtain the light absorption of the cells. The incident light is an infinite plane wave directed to the minus Z-axis of the structural unit and periodic boundary conditions are used in the in-plane directions to simulate the whole cell. A mesh-refinement of down to 1 nm was used to ensure the credibility of the simulated optical fields. For electrical simulations, basic semiconductor equations are solved on a tetragonal mesh with a fine mesh size of 1 nm, where the photocarrier-generation rate at each mesh point is determined by the optical profile from the FDTD simulations (the parasitic absorption of the ITO is considered by using a complex refractive index of the material while setting an extraction efficiency of zero in these layers). For simplicity, interface recombination is not considered and the ITO contacts are assumed to be ohmic. All simulations are performed using a commercial software package [5], which has been proven by numerous works to give a precise simulation of the device at the expense of a time-consuming process. We use $\lambda = 400$ nm incident light for the simulations while separately varying the period (P), the diameter (D) and the height (H) to reveal the underlying mechanism more clearly. Then we make the calculation for the whole short-wavelength range ($\lambda \sim 330$–450 nm) while keeping P, D and H fixed at a set of basic values depending on the former simulations. All optical and electrical parameters used in the simulations are taken from the literature [6, 7].

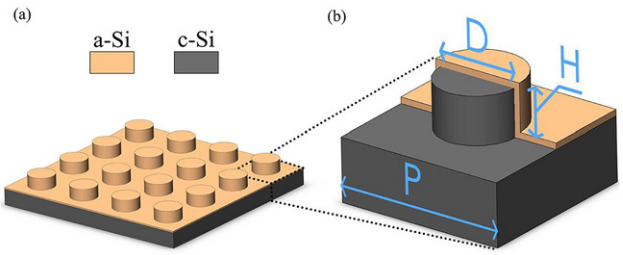

Figure 1. (a) Schematic 3D drawing of the NP HJ cells (the front and rear contacts are omitted). (b) The structural unit of the cells. The parameters D and H denote the dimensions of the c-Si core and P denotes the array period.

3. Results and discussion

3.1. NP arrays with varying period (P)

Firstly, the response of the a-Si/c-Si HJ cells versus varying NP-array period has been calculated, with fixed NP diameter ($D = 150$ nm), height ($H = 75$ nm) and incident light wavelength ($\lambda = 400$ nm). The optical (reflection) and electrical (IQE, J_{sc}) results are shown in figures 2(a) and (b), respectively. (Note that we have chosen IQE rather than external quantum efficiency (EQE). While EQE represents the combined influence of the optical and electrical properties, IQE depends exclusively on the electrical properties of the cell and thus functions as a more straightforward indicator of this effect.) For the optics, the NP arrays show excellent AR properties as compared to planar or textured surfaces [8], given that $P < \lambda$ is satisfied, as indicated in figure 2(a). A common explanation is that the NP layer has an intermediate effective refractive index which suppresses the reflection and provides better impedance matching when $P < \lambda$ [9]. Another mechanism, which is unique in nano-scale structures, is that the NPs serve as light-confining nano-cavities, and the substrate beneath them provides a leaky channel and effectively couples the light energy into the cell [9].

Then we turn to focus on the carrier-extraction capability of the cells indicated by IQE in figure 2(b). The IQE of a planar HJ cell is also shown for comparison. Notably, the IQE curve of the NP cells exhibits a sharp peak at around $P = 315$ nm, with a maximum value of 80.98%. This is over 71% higher than that of a planar HJ cell (47.32%) and corresponds to a 3-fold reduction in recombination-induced current loss. In order to interpret the gain in IQE, we refer to the light distribution profiles within these cells under $\lambda = 400$ nm illumination. As depicted in figure 3, the electric field intensities are drawn with logarithmic color scale for a planar cell and three NP cells with $P = 250$ nm/315 nm/450 nm, respectively. The dotted white lines indicate the a-Si/c-Si interfaces. Apparently, the light energy is mostly concentrated in the surface a-Si layer for the planar cell. In the meantime, a clear resonant-like pattern is

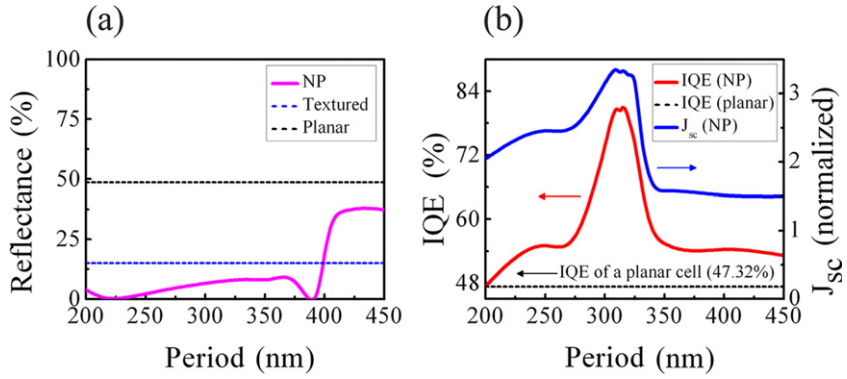

Figure 2. (a) Reflectance, (b) IQE and J_{sc} (normalized to the planar HJ cell) of the NP cells versus the NP-array period (P). The parameters D, H and λ are fixed at 150 nm, 75 nm and 400 nm, respectively.

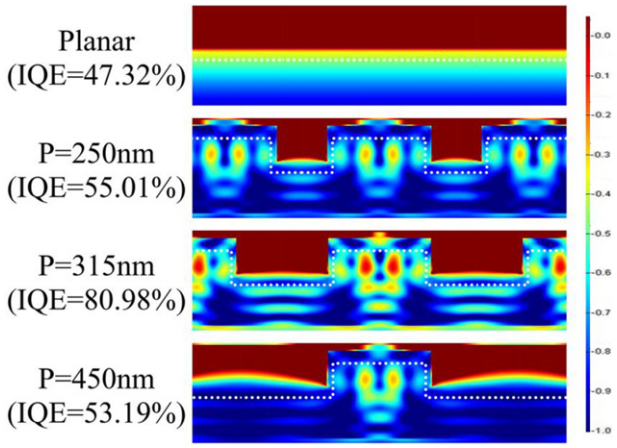

Figure 3. The light distribution profiles within the planar cell and the NP cells ($P = 250$ nm, $P = 315$ nm and $P = 450$ nm). The parameters D, H and λ are fixed at 150 nm, 75 nm and 400 nm, respectively. The dotted white lines indicate the a-Si/c-Si interfaces.

located near the center of the pillars (i.e., the c-Si region) in the NP cells. Moreover, while all three NP cells display enhanced field intensity in the c-Si region over the planar one, the light intensity inside the one with $P = 315$ nm distinctly exceeds that for $P = 250$ nm or $P = 450$ nm.

The explanation for the light distribution profile within the planar cell (or any traditionally textured cell with $\sim$10 μm feature size) is that the a-Si material possesses a large extinction-coefficient in the short-wavelength range, and thus induces strong parasitic absorption [4]. Since the carrier-generation rate is proportional to local field intensity, most carriers in the planar cell are generated in the a-Si layer. Nevertheless, the carrier-extraction probability within this layer is approximately zero, due to the insufficient carrier diffusion length caused by the defect-rich nature of the doped a-Si material [4, 10]. This inability to extract the photogenerated carriers severely deteriorates the J_{sc} of the planar cell and is reflected by the low IQE, as shown in figure 2(b), consistent with experimental observations. However, in the NP cells, the light distribution profiles are greatly modulated by the presence of the NP arrays. This is due to the fact that the NPs act as nano-cavities for light, confining and localizing light within the c-Si region [9, 11, 12]. The Q factor of this structure is estimated to be $\sim$10, which explains the highly amplified electric field intensity in the NPs [12]. As a result, the light-absorption and carrier-generation front in the NP cells is effectively shifted to the c-Si bulk region, where the carrier-extraction probability is close to unity [4, 10]. This tremendously improves the J_{sc} of the NP cells and is reflected by the significant gain in IQE.

Besides, the stronger field intensity within the $P = 315$ nm cell implies that a larger portion of light energy is absorbed by the c-Si bulk than in the cases of $P = 250$ nm or $P = 450$ nm. This is also evidenced by the strong peak at $P = 315$ nm in figure 2(b), while at other positions the IQE curve shows only moderate enhancement. This phenomenon can be explained by the excitation of guided resonance modes with suitable lattice period, in which the coupling of incident light into high-Q leaky modes of the array leads to strongly amplified field intensities inside the c-Si core of the NPs [12, 13]. Considering this together with the behavior of the IQE curve, we conclude that an array period of 315 nm best intensifies the cavity resonance and is suitable for later investigations.

3.2. NP arrays with varying diameter (D)

Secondly, the response of the a-Si/c-Si HJ cells versus varying NP diameter has been calculated, with fixed array period ($P = 315$ nm), NP height ($H = 75$ nm), and incident light wavelength ($\lambda = 400$ nm). The optical and electrical results are shown in figures 4(a) and (b), respectively. For the optics, the reflectance of the NP cells first decreases with increasing D, reaching a minimum at $D = 190$ nm, and then begins to slightly increase again, as shown in figure 4(a). The dependence of the anti-reflection property on pillar diameter is dominated by two physical factors. First, as mentioned above, an important mechanism that provides anti-reflection in NP arrays is the coupling of the resonantly confined light energy into the substrate. This imposes a strong link between the AR property and the NP diameter since only a large enough NP diameter can support guided modes for $\lambda = 400$ nm and there exists an optimal value of pillar diameter that best intensifies the resonance [12, 13]. Second, the pillar diameter determines the volume-percentage of the Si material in the NP layer. Thus, it

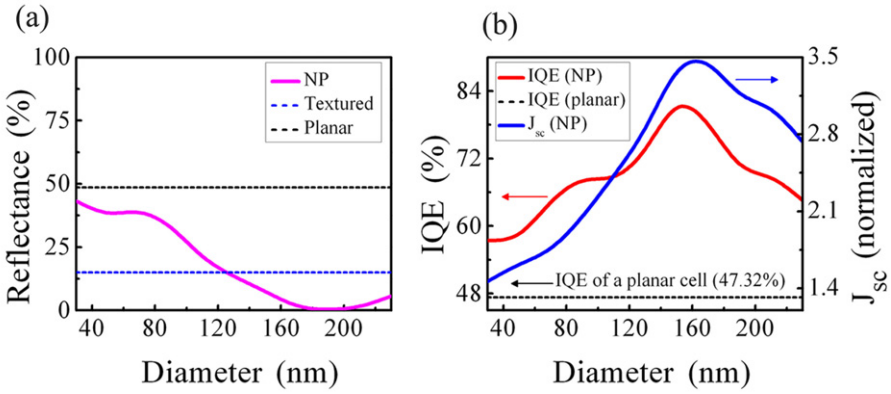

Figure 4. (a) Reflectance, (b) IQE and J_{sc} (normalized to the planar HJ cell) of the NP cells versus NP diameter (D). The parameters P, H and λ are fixed at 315 nm, 75 nm and 400 nm, respectively.

influences the effective refractive index of the layer and its AR performance.

When we compare the cell's optical performance with its carrier-extraction capability characterized by IQE in figure 4(b), we find certain similarities between the behaviors of these two distinct aspects. Generally, the IQE first increases and then decreases with increasing diameter, a similar trend to that of the AR performance. However, the IQE curve peaks at $D = 150$ nm, slightly different from the optimal value of $D = 190$ nm in anti-reflection. As discussed above, the increasing part of the IQE curve indicates that a growing proportion of carriers are generated within the c-Si region. This is a direct consequence of the strengthened excitation of wave-guiding modes [12, 13] with suitable cavity diameter, which amplifies the field intensity inside the c-Si core and thus promotes the carrier-extraction efficiency of the cell. Besides, this same mechanism also contributes to anti-reflection, which likely explains their similar dependence on pillar diameter. The discrepancy in their respective optimal values is attributed to the second factor that influences the AR performance, i.e. the effective refractive index. For silicon material ($n = 5.57$ at $\lambda = 400$ nm), an NP array functions as an optimal anti-reflection coating ($n = 2.36$) when $D = 230$ nm. This explains the peak shifting ($D = 190$ nm) observed in figure 4(a). Finally, as a product of optical absorption and electrical extraction, the J_{sc} shows its peak position at an intermediate D value of 165 nm.

3.3. NP arrays with varying height (H)

Thirdly, the response of the a-Si/c-Si HJ cells versus varying NP height has been calculated, with fixed array period ($P = 315$ nm), NP diameter ($D = 150$ nm) and incident light wavelength ($\lambda = 400$ nm). The optical and electrical results are shown in figures 5(a) and (b), respectively. Similarly to figure 4(a), the reflectance first decreases and then increases with increasing H. In this case, the behavior of the anti-reflection property is apparently dominated by the intensity of the cavity resonance, since the NP height no longer influences the effective refractive index of the layer. It has also been reported that excessive NP height weakens the cavity-resonance effect [14], which could explain the increase in reflectance for $H > 85$ nm.

In figure 5(b), substantial improvement in carrier-extraction efficiency is observed for NP height between 60 and 100 nm, indicating an effective shifting of the absorption zone with intensified resonance. This range of NP height also coincides with that in figure 5(a), where the reflectance is reduced below the texturing limit, further proving that they have originated from the same physical mechanism. The minimum in reflectance and the maximum in IQE are found at very close values of H (75 nm and 82 nm, respectively), suggesting an optimal cavity length for light resonance. This is consistent with the conclusions made in previous works [14]. Finally, the J_{sc} peaks at $H = 77$ nm under the influence of both the optical and the electrical factors.

3.4. Spectral responses in the short-wavelength range for fixed array dimensions

So far we have shown that the carrier-extraction efficiency of the a-Si/c-Si solar cell can be significantly enhanced by modulating the surface light field with NP arrays. To fully assess its capability in reducing current loss, we now calculate the short-wavelength ($\lambda \sim 330$–450 nm) spectral response of the NP cell and compare it to that of traditional ones. In these calculations we have chosen a set of parameters $P = 315$ nm/$D = 150$ nm/$H = 75$ nm according to the maxima in IQE (rather than in J_{sc}), since we want to emphasize the reduction of the electrical loss that limits the performance of a-Si/c-Si solar cells.

For the optics, the reflectance of the NP cell is shown in figure 6(a). The NP array provides better anti-reflection as compared to a textured surface in most parts of this spectral range. However, when further incorporating AR coatings, both techniques can result in a very low reflectance in a wide wavelength range [9, 15]. Thus, in real practice the optical loss is not the main source of current loss for this type of cell. In figure 6(b), we have plotted the IQE of the NP cell and that of the planar cell in the short-wavelength range. As shown by the black line, the planar cell exhibits poor carrier-extraction efficiency in this spectral range, indicating a large current loss induced by carrier recombination. By contrast, a significant gain in IQE is observed for the NP cell, as shown by the red line.

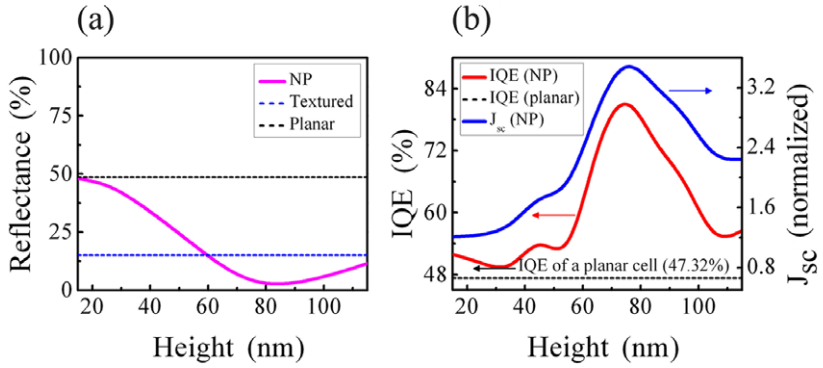

Figure 5. (a) Reflectance, (b) IQE and J_{sc} (normalized to the planar HJ cell) of the NP cells versus NP height (H). The parameters P, D and λ are fixed at 315 nm, 150 nm and 400 nm, respectively.

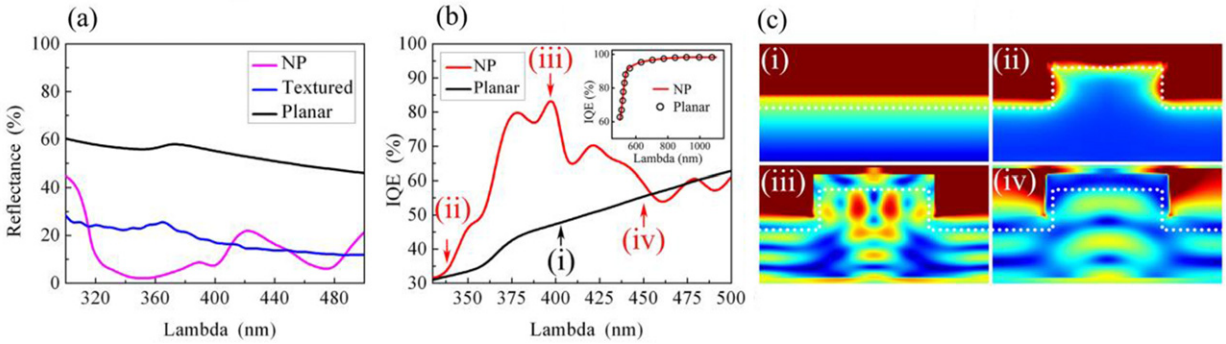

Figure 6. (a) Reflectance and (b) IQE of the optimal NP cell ($P = 315$ nm/$D = 150$ nm/$H = 75$ nm) in the short-wavelength range. Inset: IQE comparison for longer wavelengths (500–1100 nm) between the optimal NP cell and the planar cell. (c) The light distribution profiles within the planar cell and the NP cell under different illumination: (i) planar, $\lambda = 400$ nm; (ii) NP, $\lambda = 330$ nm; (iii) NP, $\lambda = 400$ nm; (iv) NP, $\lambda = 450$ nm.

Its average IQE has risen to 62.88% from the 43.94% of the planar cell, with a maximum value exceeding 80%. To estimate the gain in current, we integrate the IQE curves with the AM1.5 solar spectrum, and a total current gain of 38.25% results for this wavelength range. Compared to common cases where the J_{sc} increase comes from optical light-trapping, this 38.25% gain in current is attributed to the substantially improved carrier-extraction capability of the cell with modulated light fields. For longer wavelengths (500–1100 nm), the IQEs of both the NP cell and the planar cell rise rapidly with increasing wavelength, taking almost identical values after 500 nm, as is indicated by the inset of figure 6(b). This is due to the rapidly decreasing absorptance of the a-Si material with increasing wavelength, and apparently the absorption in the 10 nm a-Si window layer becomes almost negligible in this spectral range. (Note that at certain wavelengths around 460 and 490 nm, the IQE of the NP cell is slightly less than the planar one by about 5%, which might have originated from the increased volume of a-Si in the NP cell. However, integrating this with the AM1.5 spectrum shows little influence on the absolute gain in current.) Finally, we should note that we have chosen $\lambda = 400$ nm when optimizing the array dimensions, thus the IQE peak position is found at $\lambda = 400$ nm where the cavity resonance is most suitably intensified. Further choices of this central wavelength may result in even higher overall gains.

More detailed properties related to the IQE are indicated by the light distribution profiles versus the incident wavelength (shown in figure 6(c)), corresponding to different positions of the IQE curves in figure 6(b). Four examples are given, namely (i) the planar cell at $\lambda = 400$ nm, (ii) the NP cell at $\lambda = 330$ nm, (iii) the NP cell at $\lambda = 400$ nm and (iv) the NP cell at $\lambda = 450$ nm. The electric field intensities are drawn with logarithmic color scale, with dotted white lines indicating the a-Si/c-Si interfaces. Example (i) represents the general behavior of the planar cell under short-wavelength illumination: carriers are mostly generated in the a-Si layer and low IQE results, as shown in figure 6(b). However, for the NP cell, the light distribution pattern strongly varies with different incident wavelengths. For (ii), $\lambda = 330$ nm, the light is off-resonance and its energy submits to a quasi-exponential distribution, with most absorption taking place in the a-Si region. Similarly to the planar case, low IQE results, as indicated by the left end of the IQE curve. For (iii), $\lambda = 400$ nm, strong resonance occurs with the excitation of guided resonance modes. The effective localization of light within the c-Si region leads to the maximum IQE in figure 6(b). For (iv), $\lambda = 450$ nm, some resonance still exists, nevertheless, with a significantly weakened intensity. This corresponds to the lowering of IQE in figure 6(b).

4. Conclusion

In this work, we have demonstrated a significantly enhanced carrier-extraction capability of the a-Si/c-Si HJ solar cell with NP-induced optical modulation. This improvement is attributed to the effective localization of the light energy within the c-Si bulk, and is found to have originated from a similar physical mechanism to the AR effect, i.e. the cavity resonance. Consequently, the IQE of the NP cell increases from below 50% to over 80% at certain wavelengths, and the cell is able to collect 38.25% more current than a planar HJ cell in the short-wavelength range of 330–450 nm. These results have shown a new approach to suppressing the recombination-induced current loss in certain types of cells, without having to change the electrical properties of the materials.

Acknowledgments

This work was supported by National Major Basic Research Projects (2012CB934302 and 2011AA050502) and the Natural Science Foundation of China (11174202, 11204176, and 61234005).

References

[1] Bozzola A, Liscidini M and Andreani L C 2012 Photonic light-trapping versus Lambertian limits in thin film silicon solar cells with 1D and 2D periodic patterns *Opt. Express* **20** 224–44

[2] Ji L and Varadan V V 2012 A blazed grating for light trapping in a-Si thin-film solar cells *J. Opt.* **14** 095001

[3] Basore P A 1993 Extended spectra analysis of IQE *Photovoltaic Specialists Conf.* pp 147–152

[4] Holman Z C, Descoeudres A, Barraud L, Fernandez F Z, Seif J P, Wolf S D and Ballif C 2012 Current losses at the front of silicon heterojunction solar cells *IEEE J. Photovolt.* **2** 7–15

[5] FDTD Solutions v8 and DEVICE v3 (Lumerical, 2013)

[6] Palik E D 1998 *Handbook of Optical Constants of Solids* vol 3 (New York: Academic) pp 561–9 and 575–86

[7] Datta A, Rahmouni M, Nath M, Boubekri R, Cabarrocas P R I and Chatterjee P 2010 Insights gained from computer modeling of heterojunction with instrinsic thin layer 'HIT' solar cells *Sol. Energy Mater. Sol. Cells* **94** 1457–62

[8] Rosa M, Allegrezza M, Canino M, Summonte C and Desalvo A 2011 TMAH-textured, a-Si/c-Si, heterojunction solar cells with 10% reflectance *Sol. Energy Mater. Sol. Cells* **95** 2987–93

[9] Spinelli P, Verschuuren M A and Polman A 2012 Broadband omnidirectional antireflection coating based on subwavelength surface Mie resonators *Nature Commun.* **3** 692

[10] Jensen N, Rau U, Hausner R M, Uppal S, Oberbeck L, Bergmann R B and Werner J H 2000 Recombination mechanisms in amorphous silicon/crystalline silicon heterojunction solar cells *J. Appl. Phys.* **87** 2639–45

[11] Sanatinia R, Awan K M, Naureen S, Anttu N, Ebraert E and Anand S 2012 GaAs nanopillar arrays with suppressed broadband reflectance and high optical quality for photovoltaic applications *Opt. Mater. Express* **2** 1671–9

[12] Lin C X and Povinelli M L 2009 Optical absorption enhancement in silicon nanowire arrays with a large lattice constant for photovoltaic applications *Opt. Express* **17** 19371–81

[13] Anttu N and Xu H Q 2010 Coupling of light into nanowire arrays and subsequent absorption *J. Nanosci. Nanotechnol.* **10** 7183–7

[14] Zhang R Y, Shao B, Dong J R, Zhang J C and Yang H 2011 Absorption enhancement analysis of crystalline Si thin film solar cells based on broadband antireflection nanocone grating *J. Appl. Phys.* **110** 113105

[15] Kinoshita T, Fujishima D, Yano A, Ogane A, Tohoda S, Matsuyama K, Nakamura Y, Tokuoka N, Kanno H and Sakata H 2011 The approaches for high efficiency hit solar cell with very thin ($<100\ \mu$m) silicon wafer over 23% in *26th EUPVSC (Hamburg)* pp 871–874